

Energy occupation of waves and structures in 3D compressive MHD turbulence

L. P. Yang,^{1,2★} H. Li,^{2★} S. T. Li,² L. Zhang,¹ J. S. He³ and X. S. Feng¹

¹*SIGMA Weather Group, State Key Laboratory for Space Weather, National Space Science Center, Chinese Academy of Sciences, 100190, Beijing, China*

²*Theoretical Division, MS B284, Los Alamos National Laboratory, Los Alamos, NM 87545, USA*

³*School of Earth and Space Sciences, Peking University, 100871 Beijing, China*

Accepted 2019 June 19. Received 2019 June 16; in original form 2019 April 23

ABSTRACT

Structures and propagating waves are often observed in solar wind turbulence. Their origins and features remain to be uncovered. In this work, we use 3D driven, compressible MHD turbulence simulations to investigate the global signatures of the driven fluctuations in whole spatial and temporal domain. With four-dimensional spatial-temporal (x, y, z, t) Fourier transformations implemented, we have identified two distinct main populations: waves, which satisfy the $\omega - k$ dispersion relations and are propagating; and structures, which satisfy the polarization relations but non-propagating ($\omega = 0$). Whereas the overall turbulent energy spectrum is still consistent with $k^{-5/3}$, the contributions from waves and structures show very different behaviour in k space, with structures dominating at small k but waves becomes comparable to structures at large k . Overall, the fluctuations in the directions perpendicular to the large-scale mean field \mathbf{B}_0 are a manifestation of structures, while along the parallel direction, the fluctuations are dominated by waves. Also, a significant portion of the incompressible structures are the Alfvénic nature, and with imbalanced increased, the waves predominantly propagate in one direction and nearly perpendicular to \mathbf{B}_0 . Differentiating the relative contributions from waves and structures could have important implications for understanding the non-linear cascade processes in the inertial range as well as particle-fluctuation interactions at small scales.

Key words: MHD – turbulence – waves – methods: numerical.

1 INTRODUCTION

The solar wind, a supersonic and super-Alfvénic plasma flow, continuously expands from the Sun into the heliosphere, and is permeated by various kinds of fluctuations. Since the beginning of the space era, studying the properties of these fluctuations has been among the major research topics in solar wind physics as they play a relevant role in solar wind generation, high-energy particles acceleration, plasma heating, cosmic rays propagation, and other aspects of plasma behaviour in space (Goldstein, Roberts & Matthaeus 1995; Tu & Marsch 1995; Biskamp 2003; Bruno & Carbone 2013; Howes & Nielson 2013). In recent years, considerable progress has been made; however, the nature of the fluctuations has not yet been fully understood.

Both a well-defined turbulence spectrum and a strong correlation between velocity and magnetic fluctuations are observed in the solar wind (Coleman 1968; Belcher & Davis 1971; Burlaga & Turner 1976; Dobrowolny, Mangeney & Veltri 1980; Marsch et al.

1981; Bavassano et al. 1982; Matthaeus & Goldstein 1982; Bruno, Bavassano & Villante 1985; Roberts et al. 1987a,b; Bavassano & Bruno 1989; Grappin, Velli & Mangeney 1991; Carbone 1994; Bieber, Wanner & Matthaeus 1996; Goldstein & Roberts 1999; Bavassano, Pietropaolo & Bruno 2000; Podesta, Roberts & Goldstein 2007; Alexandrova et al. 2008; Horbury, Forman & Oughton 2008; Podesta 2009; Boldyrev et al. 2011; Li et al. 2011; Yao et al. 2013; Zhao et al. 2014; He et al. 2015; Shi et al. 2015; Wang et al. 2016; Shi et al. 2017). Two perspectives have come to dominate the view of solar wind magnetic and velocity fluctuations. Coleman (1968) found solar wind magnetic fluctuations often exhibit power laws in wavenumber k , with spectral indices close to that predicted by Kraichnan (1965), and gave first evidences that the solar wind is a highly turbulent, non-linear medium. In another pioneering paper by Belcher & Davis (1971), velocity and magnetic field fluctuations were shown to behave as pure Alfvén waves propagating outward, and since then, it has been assumed that the solar wind may be regarded as a superposition of linear waves, primarily in Alfvén modes. The turbulence description and the wave description can have different consequences, since the presence of Alfvén waves renders non-linear transfer to small scales

* E-mail: lpyang@swl.ac.cn (LPY); hli@lanl.gov (HL)

less efficient, leading to a different turbulent behaviour from that described by Kolmogorov (1941) (Kraichnan 1974). Meanwhile ubiquitous Alfvénic correlations in the solar wind have stimulated a lengthy debate based on whether the highly Alfvénic fluctuations are passive remnants of coronal processes or represent dynamically evolving turbulent magnetofluid (Matthaeus & Zhou 1989).

Meanwhile, the solar wind fluctuations mix with non-propagating coherent structures, which are often observed and are an important ingredient of the dynamics and dissipation of the solar wind fluctuations (Tu, Marsch & Thieme 1989; Bruno & Bavassano 1991; Tu & Marsch 1993; Bruno et al. 2001; Sorriso-Valvo, Carbone & Bruno 2005; Greco et al. 2009; Wang et al. 2013; Chen et al. 2014; Yang et al. 2015; Perrone et al. 2016, 2017; Roberts et al. 2017; Yang et al. 2017b,c, 2018a; Wang et al. 2018; Roberts, Narita & Escoubet 2018). In addition, non-linearly interacting fluctuations are expected to generate coherent structures (Matthaeus et al. 2015), which are interpreted as current sheets, discontinuities, shocks, magnetic solitons, magnetic holes, Alfvén vortex, and so on. Including convective structures in a turbulence model seems necessary to explain why the magnetic energy fluctuation is greater than the kinetic energy fluctuation, and the reduction of the Alfvénicity of the fluctuations with radial distance (Tu & Marsch 1993). By a statistical analysis, Bruno et al. (2007) showed that magnetically dominated structures represent an important component of the interplanetary fluctuations within the MHD range of scales.

However, no general consensus presently exists within the community regarding the nature of plasma fluctuations along the turbulent cascade. Should plasma fluctuations be viewed as a superposition of interacting waves, such as Alfvén waves at MHD scales (Gosling et al. 2009), or as a collection of coherent structures, responsible for intermittency (Groselj et al. 2018), or as a coexistence of both waves and structures (Dmitruk & Matthaeus 2009; Parashar et al. 2010; Lugones et al. 2016; Perrone et al. 2016; Andrés et al. 2017)

Wave number and frequency fluctuations together can provide important insights in answering these questions as the propagation of waves satisfies dispersion relationships, while structures will not propagate. Observationally, it is quite difficult to obtain fully four-dimensional (4D; 3D spatial plus temporal) information about the solar wind fluctuations, which makes it impossible to specify unambiguously the distribution of fluctuation energy over the full space of wave vector and frequency. In this work, we will use numerical simulations to investigate turbulent power over the full space of wave vector and frequency, especially for both waves and structures in compressive MHD turbulence with a large-scale mean magnetic field.

In Yang et al. (2018b), the polarization of MHD modes was used to decompose turbulent velocity and magnetic fields into Alfvén modes, slow modes, and fast modes, and then the time variations of the values at a strip along z -direction is examined to diagnose waves and structures. This method not only tells us the existence of waves and structures in local spots of turbulent fields, but also inspires us to see the global signatures of the driven fluctuations in whole domain (whole wavenumbers and whole frequencies. Here, with 4D spatial-temporal (x, y, z, t) Fourier transformations employed, we explore the nature of the driven fluctuations by their power distributions in the planes perpendicular and parallel to the large-scale mean field and their spectral behaviours in different wavenumber directions. Beyond these, we compute energy occupation of waves and structures, and uncover their properties, which are not illustrated before as far as we know. The paper is organized as follows: In Section 2, we describe our numerical simulation parameters. In Section 3, we

present our findings, and in Section 4, we summarize our key results and discuss their implications.

2 NUMERICAL MHD MODEL

The description of the 3D compressible MHD model we used in this paper follows the details given in Yang et al. (2017a, 2018b), where we numerically solved the 3D compressible MHD equations with a finite magnetic resistivity of $\eta = 0.0001$ and fluid viscosity of $\nu = 0.0001$. For the equation of state we choose an adiabatic index $\gamma = 5/3$. The uniform large-scale field \mathbf{B}_0 is imposed in the z -direction. We consider periodic boundary conditions in a cube with a side length of $2\pi L_0$ and a resolution defined by the number of grid points which is 512^3 .

Turbulence is driven at large scales with properties described in Yang et al. (2017a, 2018b). In particular, we have studied three cases that correspond to vary the cross-helicity σ_c while keeping the rest of turbulence parameters little changed. The base case has the following properties: the initial quantities are given as $\rho_0 = 1.00$, $|B_0| = 1.00$, and $\beta_0 = 1.00$. For turbulence driving, the root-mean-square (RMS) amplitudes of the magnetic field (B_{rms}) and velocity (u_{rms}) are maintained to be approximately 0.39 and 0.41, respectively. At the statistically quasi-stationary state (typically after tens of Alfvén times, where one Alfvén time is defined as L_0/V_A), the Mach number ($u_{\text{rms}}/\langle C_s \rangle$) ≈ 0.34 , and Alfvén Mach number (u_{rms}/V_A) ≈ 0.41 , where $\langle C_s \rangle = 1.21$ and $\langle V_A \rangle = 1$ are sonic speed and Alfvén speed, respectively. The plasma β ≈ 1.50 , and the normalized cross-helicity $\langle \sigma_c \rangle \approx 0.62$. Relative to this base case, we have studied two other cases with cross-helicity $\langle \sigma_c \rangle = 0.36$ and 0.01, respectively.

One of our key goals is to investigate how much of the turbulent fields (velocity and magnetic fields) actually come from propagating waves versus non-propagating structures. Here, we adopt a similar definition laid out in Andrés et al. (2017): using the spatial-temporal analysis of all fluctuations, those concentrated at or close to the linear dispersion relations with $\omega \neq 0$ will be called ‘waves’, while those satisfying the polarization relations of Alfvén and slow modes but with $\omega = 0$ will be called ‘structures’. Furthermore, there are fluctuations that do not satisfy either condition, which we refer as ‘residual turbulence’.

Our detailed analysis procedure is as follows: when the turbulent quantities reach a statistically quasi-stationary state, taking quantity $V_x(x, y, z, t)$ as an example, we first perform Fast Fourier transform (FFT) at each time frame to obtain $V_x^{(k)}(k_x, k_y, k_z, t)$. We then carry out mode decomposition analysis according to three basic modes in compressible MHD, i.e. fast mode (FM), slow mode (SM), and Alfvén mode (AM) using the exact relations described in Yang et al. (2018b). For example, for Alfvén mode, we get $V_{xAM}^{(k)}(k_x, k_y, k_z, t)$. Next, we perform an inverse FFT to get the perturbed quantities of each decomposed mode at each time moment in real space, e.g. $V_{xAM}(x, y, z, t)$. Finally, 4D FFT is done to obtain the energy of each decomposed mode, e.g. $V_{xAM}^{(k)}(k_x, k_y, k_z, \omega)$, over the full space of wave vector and frequency. To prevent spectral leakage induced by the non-periodicity of the time-series, a time apodization function (Hann windows) is applied prior to the 4D FFT is taken.

The time domain transform is conducted over a time duration of about 7 Alfvén time with a cadence of 0.01 Alfvén time, where one Alfvén time is defined as L_0/V_A . To realize it, after the turbulence reaches the statistically quasi-stationary state, we have stored 700 cycles on a disk with one cycle denoting one time frame. The temporal extent of the data used to perform Fourier transform is longer than one period of the Alfvén wave in the system, and the

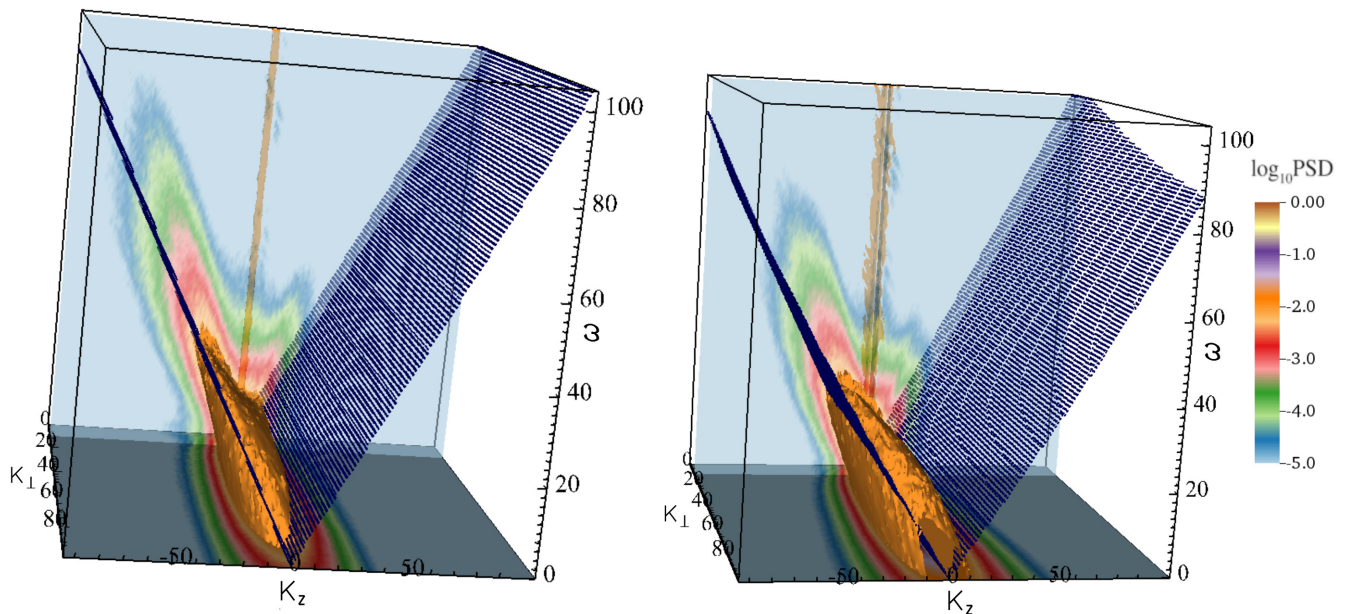


Figure 1. Distributions of PSDs of Alfvén and slow modes in the wavenumber–frequency ($k_{\perp} - k_z - \omega$) space ($u_{\text{rms}} = 0.41$, $B_{\text{rms}} = 0.39$, $\sigma_c = 0.62$, and $\beta = 1.50$). Left-hand panel: x -component of the Alfvén-mode velocity ($V_{x\text{AM}}$). Right-hand panel: z -component of the slow-mode velocity ($V_{z\text{SM}}$). The background magnetic field is in the z -direction. In both subfigures, the orange surfaces denote the iso-surface of PSDs with the value of -2.00 (as displayed in colour bar), and the blue surfaces with points show the theoretical dispersion relations of linear Alfvén (left-hand panel) and slow waves (right-hand panel) at both directions. The colours on the planes of $k_{\perp} - k_z$ with $\omega = 0$ and $k_z - \omega$ with $k_{\perp} = 15$ represent the iso-contours of PSD without projection. Both the propagating waves and the non-propagating structures ($\omega \approx 0$) are visible.

temporal data cadence is about twice as fast as the fastest wave crossing over one grid size. The longer temporal extent of the data is tested and the results converge. In our implementations, the FFT has been conducted with FFTW software (Frigo & Johnson 2005) configured to run in parallel for the huge amount of 4D data. Here we chose to run it with one process for one time frame/cycle.

It is noted that the method of 4D Fourier transform applied above differs greatly from the slicing method appeared in Yang et al. (2018b), which extracted the mode values along the direction of the mean field (z -direction), and stacked the obtained profiles in time sequence to obtain distance–time ($z-t$) or wavenumber–frequency ($k_z - \omega$) diagrams at a fixed x , y point. The information explored from the method of 4D Fourier transform are therefore far beyond that from the slicing method, which will be illustrated in the below section.

In the simulations we presented here, it turns out that the fast modes consist of a very small amount of energy (Cho & Lazarian 2002; Yang et al. 2018b), so we will present only the results on Alfvén and slow modes. Note that the mode decomposition method described in Yang et al. (2018b) will decompose *all* the velocity fluctuations into either one of the three modes, so the summation of the kinetic energies in all Alfvén, slow and fast modes will recover the total turbulent kinetic energy.

3 NUMERICAL RESULTS

We now present results concerning the waves and structures in 3D MHD compressible turbulence based on our simulations. Our primary goals include demonstrating the features of both propagating waves and non-propagating structures and their different behaviours of spectral energy density in \mathbf{k} -space in compressible MHD turbulence.

Fig. 1 presents the power spectral density (PSD) distributions of Alfvén and slow modes in the wavenumber–frequency ($k_{\perp} - k_z - \omega$) space for the base run, where we have used the x -component of the Alfvén-mode velocity ($V_{x\text{AM}}$) and the z -component of the slow-mode velocity ($V_{z\text{SM}}$) as representative quantities. It can be seen that the driven fluctuations behave as three apparent main features:

First, there is significant energy in the fluctuations with $\omega \neq 0$ that are associated with the Alfvén and slow waves along linear dispersion relations, indicating the evident presence of propagating Alfvén and slow waves in MHD turbulence. We refer them as ‘waves’ in the paper. This result is consistent with the previous studies by Andrés et al. (2017). For the base run with a cross helicity $\sigma_c = 0.62$, although both the forward and counter-propagating (larger power) Alfvén modes are injected at large scales, at the steady state, curiously only one-direction Alfvén and slow waves are visible from Fig. 1 (this direction is the same as the direction of the dominant injected mode).

Secondly, there is also significant energy in the fluctuations on the $k_{\perp} - k_z$ plane with $\omega \approx 0$ in both the Alfvén and slow mode components. These are non-propagating structures that display high degree of anisotropy in $k_{\perp} - k_z$ plane, and they have far more power along the direction perpendicular to the background mean magnetic field. We refer them as ‘structures’ in the paper. We also find that, for various runs with the different cross-helicity σ_c , plasma β , and Alfvén Mach number M_A , these main signatures do not change much, except that for the balanced run ($\sigma_c = 0.01$), the dual-direction waves can be seen.

Thirdly, there is energy in the fluctuations that have $\omega \neq 0$ but they do not satisfy the linear dispersion relations either. We refer them as ‘residual turbulence’ in the paper.

To further illustrate the three main features of the driven fluctuations in Fig. 1, we plot the PSD of the Alfvén-mode and slow-modes

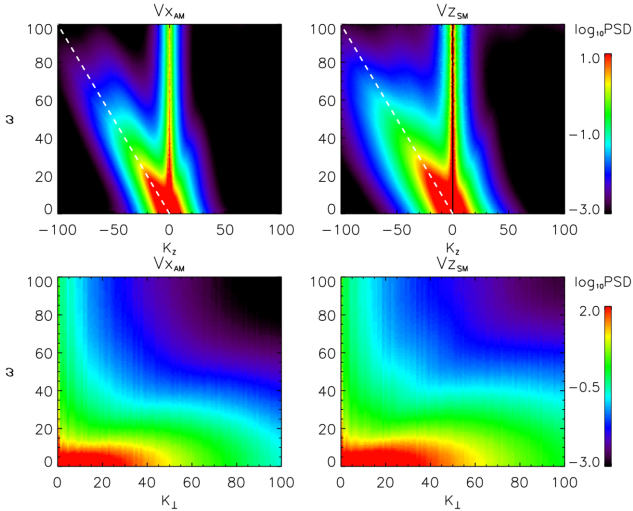


Figure 2. PSD distributions of the Alfvén-mode (left-hand panels) and slow-modes (right-hand panels) on the ω - k_z (up panels) and ω - k_\perp (low panels) planes. Dashed lines are the theoretical linear dispersion relations of Alfvén and slow waves.

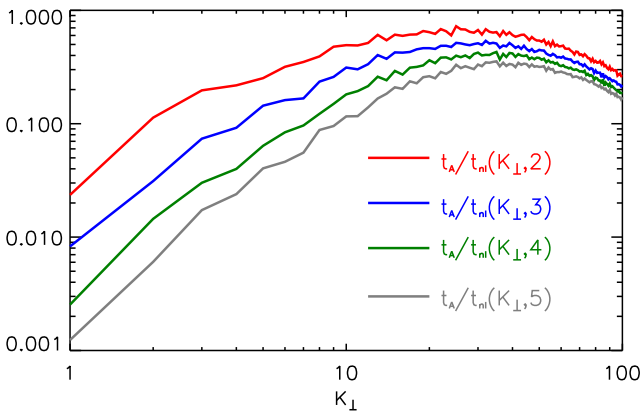


Figure 3. Time ratio t_A/t_{nl} as a function of the perpendicular wavenumber k_\perp at a given $k_z = 2, 3, 4, 5$ for the turbulent kinetic energy.

on the ω - k_z and ω - k_\perp planes in Fig. 2. These are essentially the same as summing up all the k_\perp contributions and as summing up all the k_z contributions in Fig. 1. We can see that the PSD distributions in the ω - k_z plane overlap well with the theoretical dispersion relations of linear Alfvén and slow waves, indicating that the fluctuations in the parallel direction could be viewed as a superposition of linear waves, while the PSD in the ω - k_\perp plane concentrate mainly at the small frequency, pointing out that the fluctuations in the perpendicular directions could be a manifestation of structures. It is noted that the fluctuations could behave as field-aligned waves and 2D structures in the perpendicular directions, which could not be revealed by the method in Yang et al. (2018b).

To see whether the presented numerical experiment is in the strong turbulent regime or in a mixed weak/strong regime, Fig. 3 displays the ratio t_A/t_{nl} as a function of k_\perp at a given $k_z = 2, 3, 4, 5$ for the turbulent kinetic energy, where t_A is the linear characteristic time, defined as $t_A = k_z B_0$, with B_0 being the large-scale mean field, and t_{nl} is the non-linear characteristic time, defined as $t_{nl} = k_\perp b$, with $b = \sqrt{2k_z k_\perp E^v(k_\perp, k_z)}$ and $E^v(k_\perp, k_z)$ being bi-dimensional kinetic

energy spectrum (Meyrand, Galtier & Kiyani 2016; Meyrand et al. 2018). From this figure, it can be seen that, at large scales, t_A/t_{nl} is far less than 1, suggesting that it is in the weak turbulence regime. As the scales decrease, t_A/t_{nl} increases quickly. At $k_\perp = 10$, it nearly comes to a plateau, with its value approaching unity (≥ 0.1) as k_z increases, suggesting that it is nearly in the strong turbulence regime.

Fig. 4 shows the spatial energy spectrum of turbulent kinetic energy E_k as a function of wavenumber k , k_\perp and k_z , respectively, for both Alfvén (top row) and slow (bottom row) modes, using the outputs from the base run. The wave component comes from all fluctuations in the k_\perp - k_z - ω space within an angle of 7° (both upwards and downwards) of the linear dispersion relations of Alfvén and slow waves. We have tested that with the angle greater than 7° , the results presented here converge. On the other hand, the structure component comes from all fluctuations on the plane of $\omega = 0$.

In each plot, we include three curves, which represent the PSD components of the waves (red), structures (blue), and the total (black), respectively. It can be seen that the spectrum of the total Alfvén and slow modes (black curves in the left and middle columns) follow a Kolmogorov-like $-5/3$ spectrum. Most of the power is along the k_\perp . All of these results are consistent with expectations for MHD turbulence.

One notable result from this analysis, however, is the relative contribution by structures and waves changes as a function of k . From the injection scale through most of the inertial range, the power spectra in k or k_\perp are dominated by the structures at large scales, but as k or k_\perp increases, the contribution from waves seems to become comparable with or even overtake that of structures at k (k_\perp) > 20 -30. This is due to the fact that the spectrum of the structure component is $\sim k^{-2}$, steeper than the spectrum of the wave component, which is $\sim k^{-5/3}$ for the Alfvén modes.

Fig. 4 also shows that, along the parallel wavenumber k_z , the power of the waves is dominating at all scales for both Alfvén and slow modes. This means again that, in the parallel plane the fluctuations can be thought more as waves, and in the perpendicular plane, the fluctuations can be seen as 2D structures (Matthaeus, Goldstein & Roberts 1990; Zank & Matthaeus 1992).

To demonstrate the properties of the structures and waves in compressible MHD turbulence, we now present analysis of their spatial properties in detail. We first look at the structures with $\omega = 0$. Based on the 4D spatial-temporal Fourier transform using each physical variable such as V_{xAM} , B_{xAM} , ρ , etc., we first filter their power spectra with frequency, choosing only those with $\omega = 0$. Then, an inverse Fourier transform is conducted to get the purely non-propagating structures distributed in real space. These steps were carried out for both the incompressible Alfvén-mode and compressive slow-mode structures.

The four panels of Fig. 5 display the distributions of the Alfvén-mode structures V_{xAM} , B_{xAM} , V_{yAM} , and B_{yAM} on the z - y planes. Both the strong spatial correlation between the velocity and magnetic components and the similar magnitudes of these quantities demonstrate that these $\omega = 0$ fluctuations satisfy the Alfvén-mode polarization relations. Similarly, the four panels of Fig. 6 show the distributions of the slow-mode structures V_z , B_z , B , and ρ on the x - y planes. V_z is anticorrelated with density ρ , but is correlated with B_z and the total B . These features conform to the slow-mode polarization relations, even when they are not propagating. Both Figs 5 and 8 tell us that a significant portion of the incompressible structures are Alfvénic in nature, and the compressible structures are the slow-mode nature. Furthermore, we have analysed the spatial

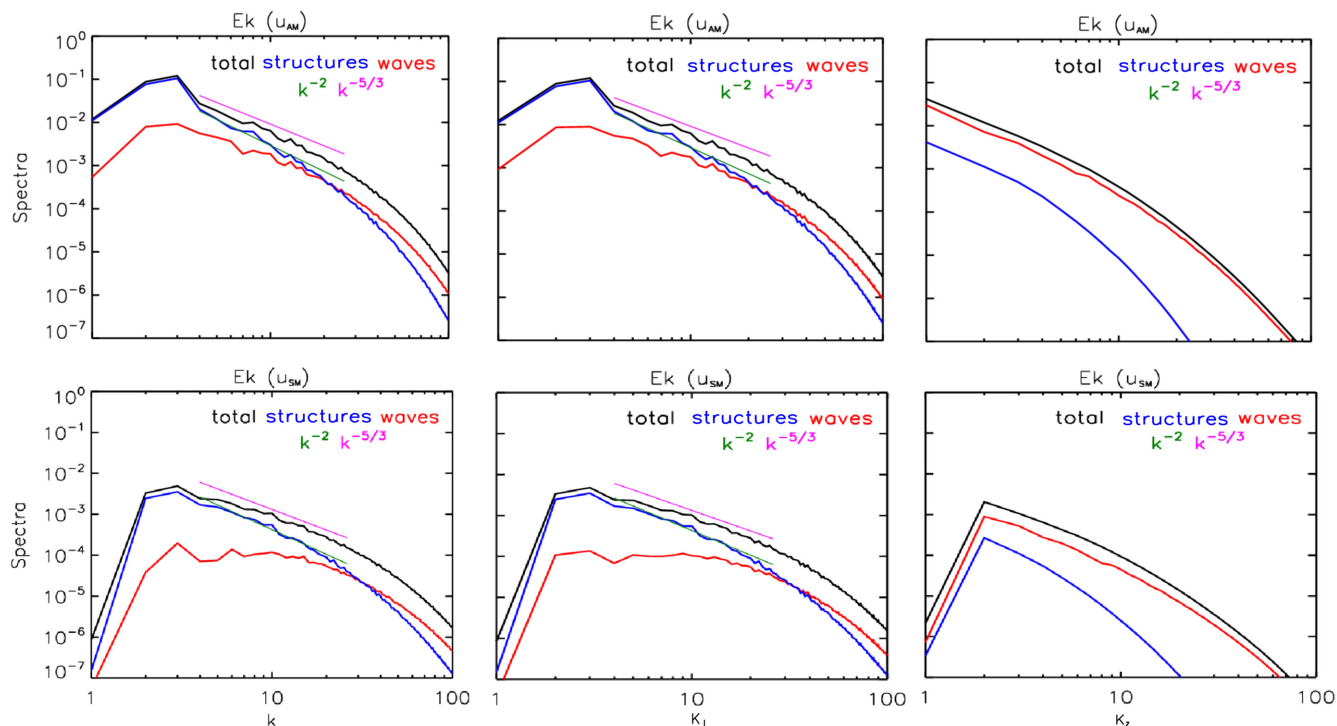


Figure 4. Spatial turbulent kinetic energy spectra as a function of the total wavenumber k (left-hand panels), perpendicular wavenumber k_{\perp} (middle panel), and parallel wavenumber k_z (right-hand panel). The upper and lower rows are for Alfvén modes (AM) and slow modes (SM), respectively. For each mode, the blue, red, and black curves show the energy in structures, in waves, and in total, respectively. For reference, $-5/3$ and -2 power-law spectra are plotted as pink and green lines, respectively.

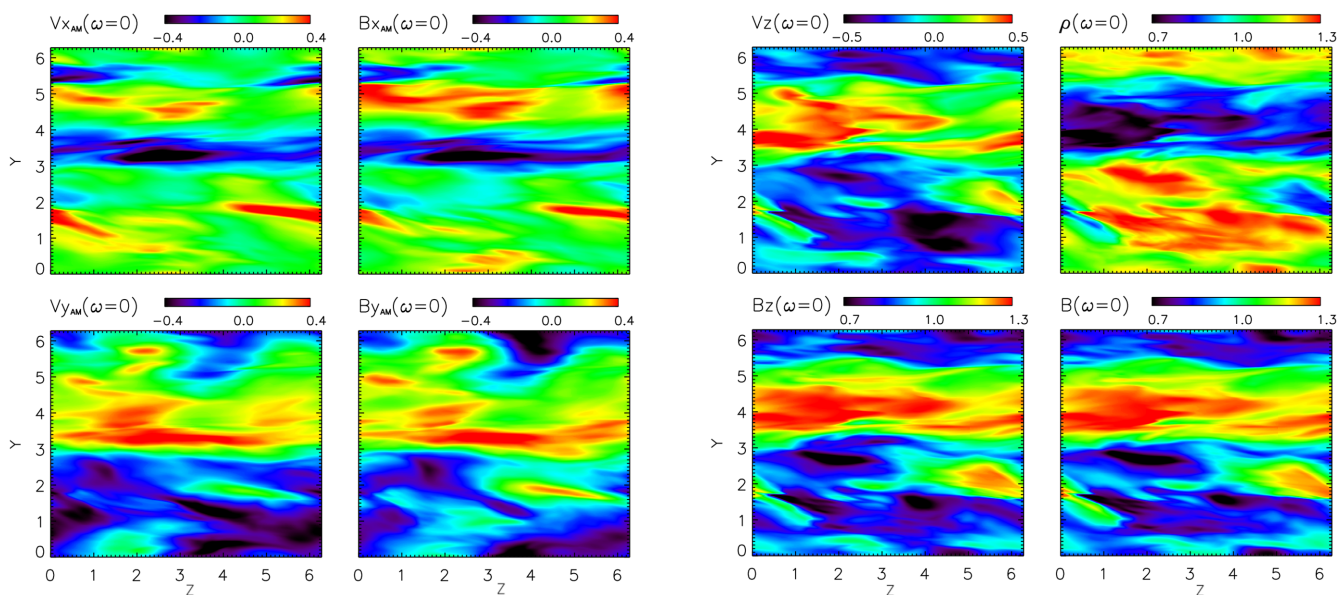


Figure 5. Spatial distributions of the incompressible Alfvén-mode structures ($\omega = 0$) shown by V_{xAM} , B_{xAM} , V_{yAM} , and B_{yAM} on the z - y plane (parallel to the mean background magnetic field).

Figure 6. Spatial distributions of the compressive slow-mode structures ($\omega = 0$) shown by V_z , ρ , B_z , and B on the z - y plane (parallel to the mean background magnetic field).

correlations for non-propagating structures in different wavenumber k ranges by using either low-pass or high-pass filters in k . We have again found high degrees of correlations, as expected. This confirms that such properties exist in both the injection range and the inertial range.

Fig. 7 shows a comparison of the Alfvén-mode velocity (V_{xAM}) among the Alfvén modes with all frequencies, Alfvén-mode structures with $\omega = 0$, and Alfvén modes with $\omega \neq 0$. The Alfvén modes with all frequencies denote a single actual picture of one state at one given time. We can see that the Alfvén-mode structures preserve

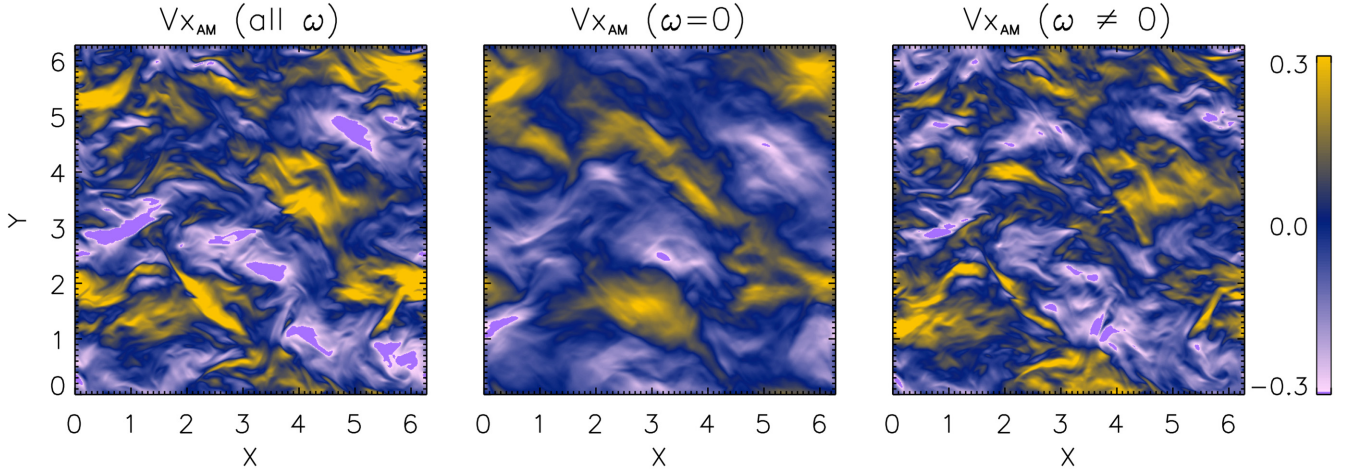


Figure 7. Spatial distributions of the Alfvén-mode velocity (V_{xAM}) for the Alfvén modes with all frequencies ω (left-hand panel), Alfvén-mode structures with $\omega = 0$ (middle panel), and Alfvén modes with $\omega \neq 0$ (right-hand panel) at an instantaneous time on the x – y plane (perpendicular to the mean background magnetic field).

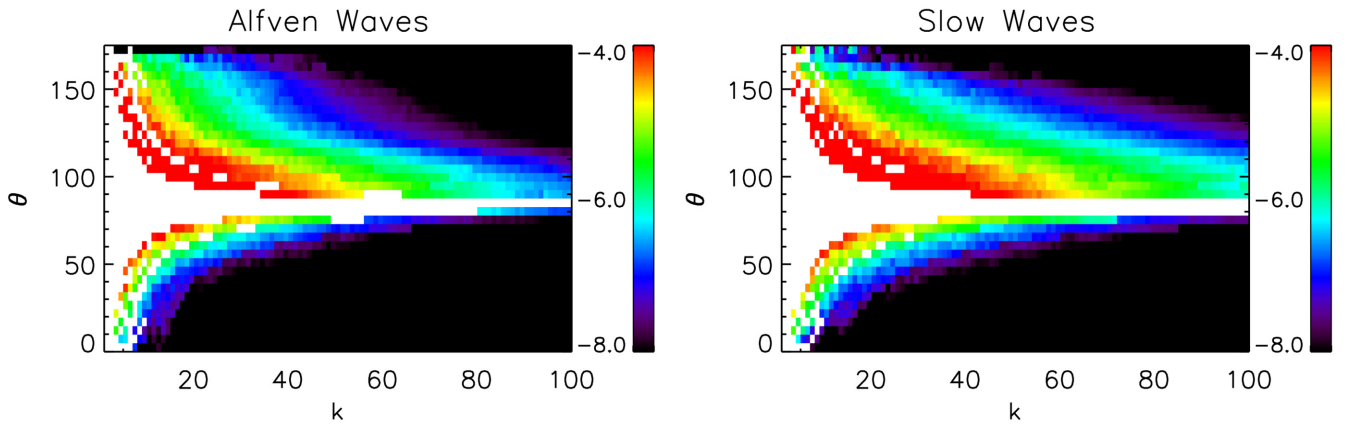


Figure 8. PSD distributions of the Alfvén-mode velocity (V_{xAM}) for the identified Alfvén waves (left-hand panel) and the slow-mode velocity (V_{zSM}) for the identified slow waves (right-hand panel) on the θ – k plane. θ is the angle between wave vector \mathbf{k} and the large-scale mean magnetic field \mathbf{B}_0 .

many of the features appeared in the total Alfvén modes. Compared with the Alfvén modes with $\omega \neq 0$, the Alfvén-mode structures behave as the large-scale structures. These results are consistent with the energy spectra distribution that the structures contribute to most of turbulence energy at the large scales, as shown in Fig. 4.

Next, we investigate how the wave propagation direction varies as a function of k . For a given wave component, we define θ as the angle between its wave vector \mathbf{k} and the large-scale mean magnetic field \mathbf{B}_0 . Using the velocity variations as the analysis variables, Fig. 8 shows the PSD distributions of the identified Alfvén and slow waves on the θ – k plane for the basic run, where we can see that the power of the identified Alfvén and slow waves mainly concentrates at the large angles to \mathbf{B}_0 . As k increases, the concentration around $\theta = 90^\circ$ is more evident, implying that most of the waves at large k are propagating nearly perpendicular to \mathbf{B}_0 . Furthermore, as k increases, the power in waves with $\theta > 90^\circ$ is much larger than that those with $\theta < 90^\circ$. This means that the identified Alfvén and slow waves at shorter wavelengths become quasi-perpendicular and are predominantly in one direction (highly imbalanced), consistent with the results shown in Fig. 1.

To further illustrate how the relative contributions from wave and structure components vary as a function of k , we have plotted the power percentage of each component separately in Fig. 9. Fig. 9 presents the power percentages of the waves and structures for the runs with the different cross-helicity σ_c . For all three cases, as wavenumber k increases, the power percentages of the Alfvén and slow waves rise quickly from about $k = 3$ to about $k = 20$, after which the power percentages of the Alfvén and slow waves keep steady. Different from these waves' behaviour, the power percentages of the Alfvén-mode and slow-mode structures drop quickly from about 80 per cent at $k = 3$ to about 20 per cent at $k = 20$. As the imbalance rises, the power percentages of the Alfvén and slow waves go up at small scales, while the power percentages of the Alfvén-mode and slow-mode structures decline.

To see wave signatures in the strong turbulence, Fig. 10 presents PSD distributions of Alfvén modes in the wavenumber–frequency space, spatial turbulent kinetic energy spectra and time ratio t_A/t_{nl} for the run with $u_{rms} = 0.62$, $B_{rms} = 0.54$, $\sigma_c = 0.42$, and $\beta = 0.38$. It shows that the turbulent kinetic energy spectra display a power law, with a slope of about $-5/3$, and the non-linear characteristic time t_{nl} is of the order of the linear characteristic time t_A beyond

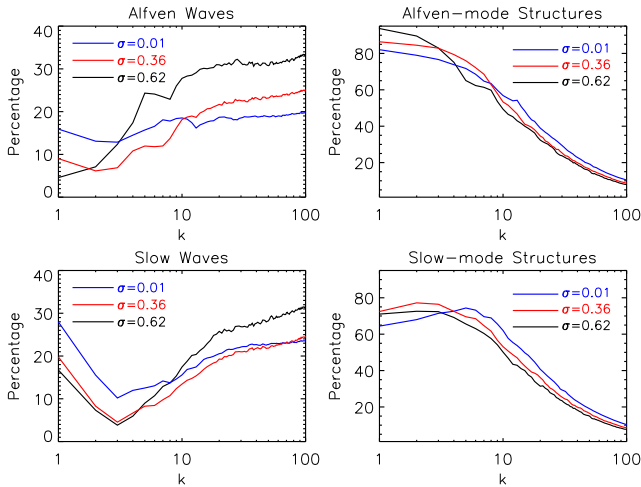


Figure 9. Power percentages of the waves and structures for the runs with different cross-helicity σ_c . Upper panels: Relative power percentage of the Alfvén waves (left) and the Alfvén-mode structures (right). Lower panels: Relative power percentage of the slow waves (left) and the slow-mode structures (right).

$k_{\perp} = 10$, suggesting that it is in the strong turbulence regime. However, wave signatures are still visible in the spatial-temporal domain, as displayed by the PSD distributions of Alfvén modes in the wavenumber–frequency space.

4 SUMMARY AND DISCUSSION

We have carried out several 3D strong, compressible MHD turbulence simulations with a large-scale mean magnetic field. Simulation runs have plasma β near unity and various cross-helicity σ_c from 0.01 to 0.62. The turbulent driving is taken to be strong with both B_{rms}/B_0 and $u_{\text{rms}}/V_A \sim 0.4$ and ~ 0.6 . At steady state, the total turbulent energy spectra reach the typical behaviour that varies as $k^{-5/3}$ with power predominantly along the k_{\perp} direction. In this paper,

we focus on separating the signatures of the propagating waves and the non-propagating structures in compressible turbulence. To realize this, the 4D Fourier transform in $x-y-z-t$ space is implemented to get the power of the perturbed velocities and magnetic fields of the Alfvén and slow modes over the full spectral domain of wave vector \mathbf{k} (k_{\perp} , k_z) and frequency ω . Here, we list our key findings:

(i) Overall, out of the total turbulent fluctuations summing over all wavenumbers, about 77 per cent are in non-propagating structures with $\omega = 0$, about 14 per cent are in propagating waves that satisfy the linear dispersion relations, and about 9 per cent are in ‘residual turbulence’, that have $\omega \neq 0$ but do not satisfy the linear dispersion relations either. In addition, the energy in Alfvén modes dominates over the energy in slow modes, and the energy in fast modes is negligible.

(ii) The PSD spectra for the Alfvén waves and structures are distinctly different. Whereas the Alfvén structures dominate at small k (k_{\perp}), they have a spectral slope $\sim k^{-2}$ versus the wave component which has a spectral slope of $\sim k^{-5/3}$. This implies that, as k (k_{\perp}) increases, the wave component becomes increasingly important. In fact, the contributions to the total power spectra from structures and waves become comparable for $k(k_{\perp}) > 20$. Very similar behaviour is observed for the slow modes, with an even flatter spectral energy distribution for the slow wave component, suggesting its dominance at large k . In addition, as the cross-helicity σ_c increases, the ratio of power in the Alfvén and slow waves over structures increases as well.

(iii) The fluctuations in the perpendicular directions are a manifestation of structures, while along the parallel direction (k_z), the fluctuations are dominated by waves.

(iv) Detailed polarization analyses show that a significant portion of the incompressible structures are the Alfvénic nature, and the compressible structures are slow mode.

(v) For the large σ_c base run, the waves with large $k(k_{\perp})$ are even more imbalanced, predominantly propagating in one direction and nearly perpendicular to \mathbf{B}_0 .

The simulation is done on an unmoving frame, and the average of the resulted velocity is zero. Relative to the propagating waves, the

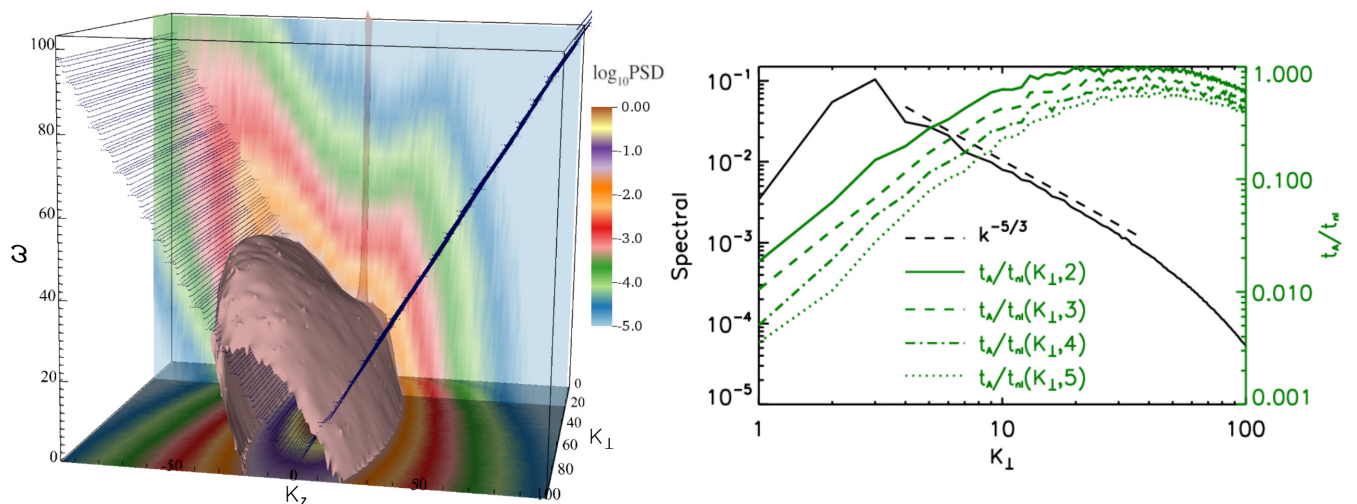


Figure 10. Left-hand panel: Same as Fig. 1 but for the strong turbulence run ($u_{\text{rms}} = 0.62$, $B_{\text{rms}} = 0.54$, $\sigma_c = 0.42$, and $\beta = 0.38$), and the isosurface of PSDs is at the value of -1.50 . Right-hand panel: Spatial turbulent kinetic energy spectra (black line) and time ratio t_A/t_{nl} (green line) as a function of the perpendicular wavenumber k_{\perp} for the strong turbulence run.

diagnosed structures are called ‘non-propagating’, which means that the frequency of the structures is zero. Actually, as the Sun rotates and the solar wind propagates outwards, the structures are comoving with the solar wind. Here, like many authors (Greco et al. 2009; Boldyrev et al. 2011; Zhdankin et al. 2012; Beresnyak 2014), we aim to see local spots of solar wind turbulence, with the simulation domain far smaller than the Solar-terrestrial distance. To approach the real state of solar wind turbulence, the expansion and propagation of solar wind may need to be considered, as Grappin & Velli (1996), Dong, Verdini & Grappin (2014), and Verdini & Grappin (2015) did.

The ‘weak turbulence’ approach postulates that turbulence might be described, in a leading order fashion, as an ensemble of waves. Here, we showed that out of the total turbulence energy, the structures with $\omega = 0$ are dominant (~ 77 per cent), which conforms to solar wind observation that about 85 per cent of the energy is in 2D component (Bieber et al. 1996), so that we could not apply the weak turbulence arguments here. Our results are also consistent with the excellent work by Parashar et al. (2010), who found that in the limit of strong turbulence, 2.5D hybrid kinetic behaviour is dominated by feature-less ‘zero frequency’ behaviour

The key results on different behaviour in spectral domain for waves and non-propagating structures need to be studied with even higher resolution simulations. The fact that both waves and structures are universal in compressible MHD turbulence is quite interesting, and it potentially provides a new perspective in understanding the non-linear cascade process through the inertial range. In particular, the increasing importance of the wave component at small scales might open up new regimes for understanding turbulence in these scales. This could have important implications for understanding particle-turbulence interactions at small scales as well.

ACKNOWLEDGEMENTS

Useful discussions with W. Matthaeus and J. Cho are gratefully acknowledged. This work is supported by NSFC grants under contracts 41774157, 41674171, 41531073, 41731067, and 41574168. HL and SL acknowledge support by LANL/LDRD and DoE/OFES programmes. Institutional Computing resources at LANL are used for all the simulations reported in this paper.

REFERENCES

Alexandrova O., Carbone V., Veltri P., Sorriso-Valvo L., 2008, *ApJ*, 674, 1153
 Andrés N., Clark di Leoni P., Mininni P. D., Dmitruk P., Sahraoui F., Matthaeus W. H., 2017, *Phys. Plasmas*, 24, 102314
 Bavassano B., Bruno R., 1989, *J. Geophys. Res.*, 94, 11977
 Bavassano B., Dobrowolny M., Mariani F., Ness N. F., 1982, *J. Geophys. Res.*, 87, 3617
 Bavassano B., Pietropaolo E., Bruno R., 2000, *J. Geophys. Res.*, 105, 15959
 Belcher J. W., Davis L. Jr, 1971, *J. Geophys. Res.*, 76, 3534
 Beresnyak A., 2014, *ApJ*, 784, L20
 Bieber J. W., Wanner W., Matthaeus W. H., 1996, *J. Geophys. Res.*, 101, 2511
 Biskamp D., 2003, *Magnetohydrodynamic Turbulence*. Cambridge Univ. Press, Cambridge, UK, p. 310
 Boldyrev S., Perez J. C., Borovsky J. E., Podesta J. J., 2011, *ApJ*, 741, L19
 Bruno R., Bavassano B., 1991, *J. Geophys. Res.*, 96, 7841
 Bruno R., Carbone V., 2013, *Living Rev. Sol. Phys.*, 10,

Bruno R., Bavassano B., Villante U., 1985, *J. Geophys. Res.*, 90, 4373
 Bruno R., Carbone V., Veltri P., Pietropaolo E., Bavassano B., 2001, *Planet. Space Sci.*, 49, 1201
 Bruno R., D’Amicis R., Bavassano B., Carbone V., Sorriso-Valvo L., 2007, *Ann. Geophys.*, 25, 1913
 Burlaga L. F., Turner J. M., 1976, *J. Geophys. Res.*, 81, 73
 Carbone V., 1994, *Ann. Geophys.*, 12, 585
 Chen C. H. K., Sorriso-Valvo L., Šafránková J., Němeček Z., 2014, *ApJ*, 789, L8
 Cho J., Lazarian A., 2002, *Phys. Rev. Lett.*, 88, 245001
 Coleman P. J. Jr, 1968, *ApJ*, 153, 371
 Dmitruk P., Matthaeus W. H., 2009, *Phys. Plasmas*, 16, 062304
 Dobrowolny M., Mangeney A., Veltri P., 1980, *Phys. Rev. Lett.*, 45, 144
 Dong Y., Verdini A., Grappin R., 2014, *ApJ*, 793, 118
 Frigo M., Johnson S. G., 2005, *Proc. IEEE*, 93, 216
 Goldstein M. L., Roberts D. A., 1999, *Phys. Plasmas*, 6, 4154
 Goldstein M. L., Roberts D. A., Matthaeus W. H., 1995, *ARA&A*, 33, 283
 Gosling J. T., McComas D. J., Roberts D. A., Skoug R. M., 2009, *ApJ*, 695, L213
 Grappin R., Velli M., 1996, *J. Geophys. Res.*, 101, 425
 Grappin R., Velli M., Mangeney A., 1991, *Ann. Geophys.*, 9, 416
 Greco A., Matthaeus W. H., Servidio S., Chuychai P., Dmitruk P., 2009, *ApJ*, 691, L111
 Grosej D., Chen C. H. K., Mallet A., Samtaney R., Schneider K., Jenko F., 2018, preprint (arXiv:1806.05741)
 He J. et al., 2015, *ApJ*, 813, L30
 Horbury T. S., Forman M., Oughton S., 2008, *Phys. Rev. Lett.*, 101, 175005
 Howes G. G., Nielson K. D., 2013, *Phys. Plasmas*, 20, 072302
 Kolmogorov A., 1941, *Akademiia Nauk SSSR Doklady*, 30, 301
 Kraichnan R. H., 1965, *Phys. Fluids*, 8, 1385
 Kraichnan R. H., 1974, *J. Fluid Mech.*, 62, 305
 Li G., Miao B., Hu Q., Qin G., 2011, *Phys. Rev. Lett.*, 106, 125001
 Lugones R., Dmitruk P., Mininni P. D., Wan M., Matthaeus W. H., 2016, *Phys. Plasmas*, 23, 112304
 Marsch E., Rosenbauer H., Schwenn R., Muehlhaeuser K.-H., Denskat K. U., 1981, *J. Geophys. Res.*, 86, 9199
 Matthaeus W. H., Goldstein M. L., 1982, *J. Geophys. Res.*, 87, 6011
 Matthaeus W. H., Zhou Y., 1989, *Phys. Fluids B*, 1, 1929
 Matthaeus W. H., Goldstein M. L., Roberts D. A., 1990, *J. Geophys. Res.*, 95, 20673
 Matthaeus W. H., Wan P., Servidio S., Greco A., Osman K. T., Oughton S., Dmitruk P., 2015, *Phil. Trans. R. Soc.*, 737, 325810107
 Meyrand R., Galtier S., Kiyani K. H., 2016, *Phys. Rev. Lett.*, 116, 105002
 Meyrand R., Kiyani K. H., Gürçan A.-z. D., Galtier S., 2018, *Phys. Rev. X*, 8, 031066
 Parashar T. N., Servidio S., Breech B., Shay M. A., Matthaeus W. H., 2010, *Phys. Plasmas*, 17, 102304
 Perrone D., Alexandrova O., Mangeney A., Maksimovic M., Lacombe C., Rakoto V., Kasper J. C., Jovanovic D., 2016, *ApJ*, 826, 196
 Perrone D., Alexandrova O., Roberts O. W., Lion S., Lacombe C., Walsh A., Maksimovic M., Zouganelis I., 2017, *ApJ*, 849, 49
 Podesta J. J., 2009, *ApJ*, 698, 986
 Podesta J. J., Roberts D. A., Goldstein M. L., 2007, *ApJ*, 664, 543
 Roberts D. A., Klein L. W., Goldstein M. L., Matthaeus W. H., 1987a, *J. Geophys. Res.*, 92, 11021
 Roberts D. A., Goldstein M. L., Klein L. W., Matthaeus W. H., 1987b, *J. Geophys. Res.*, 92, 12023
 Roberts O. W., Narita Y., Li X., Escoubet C. P., Laakso H., 2017, *J. Geophys. Res. (Space Phys.)*, 122, 6940
 Roberts O. W., Narita Y., Escoubet C.-P., 2018, *Ann. Geophys.*, 36, 527
 Shi M., Li H., Xiao C., Wang X., 2017, *ApJ*, 842, 63
 Shi M. J., Xiao C. J., Li Q. S., Wang H. G., Wang X. G., Li H., 2015, *ApJ*, 815, 122
 Sorriso-Valvo L., Carbone V., Bruno R., 2005, *Space Sci. Rev.*, 121, 49
 Tu C.-Y., Marsch E., 1993, *J. Geophys. Res.*, 98, 1257
 Tu C.-Y., Marsch E., 1995, *Space Sci. Rev.*, 73, 1
 Tu C.-Y., Marsch E., Thieme K. M., 1989, *J. Geophys. Res.*, 94, 11739
 Verdini A., Grappin R., 2015, *ApJ*, 808, L34

- Wang X., Tu C., He J., Marsch E., Wang L., 2013, *ApJ*, 772, L14
- Wang T., Cao J., Fu H., Meng X., Dunlop M., 2016, *Geophys. Res. Lett.*, 43, 1854
- Wang X., Tu C.-Y., He J.-S., Wang L.-H., Yao S., Zhang L., 2018, *J. Geophys. Res.*, 123, 57
- Yang L. et al., 2015, *ApJ*, 809, 155
- Yang L. et al., 2017a, *ApJ*, 836, 69
- Yang L., He J., Tu C., Li S., Zhang L., Wang X., Marsch E., Wang L., 2017b, *ApJ*, 846, 49
- Yang L., Zhang L., He J., Tu C., Li S., Wang X., Wang L., 2017c, *ApJ*, 851, 121
- Yang L., Zhang L., He J., Tu C., Li S., Wang X., Wang L., 2018a, *ApJ*, 855, 69
- Yang L., Zhang L., He J., Tu C., Li S., Wang X., Wang L., 2018b, *ApJ*, 866, 41
- Yao S., He J.-S., Tu C.-Y., Wang L.-H., Marsch E., 2013, *ApJ*, 774, 59
- Zank G. P., Matthaeus W. H., 1992, *J. Geophys. Res.*, 97, 17
- Zhao J. S., Voitenko Y., Yu M. Y., Lu J. Y., Wu D. J., 2014, *ApJ*, 793, 107
- Zhdankin V., Boldyrev S., Mason J., Perez J. C., 2012, *Phys. Rev. Lett.*, 108, 175004

This paper has been typeset from a $\text{\TeX}/\text{\LaTeX}$ file prepared by the author.